(Received 14 March 2025, Accepted 21 April 2025, Scheduled 28 April 2025)

A Dual-Polarized Broadband Magneto-Electric Dipole Antenna Incorporating Parasitic Elements

Xinyi Li[1,2], Wusheng Ji[1,2,*], Haibo Li[1,2], and Jingbo Shi[1,2]

[1] *Institute of Antenna and Microwave Techniques, Tianjin University of Technology and Education, Tianjin 300222, China*
[2] *School of Electronic Engineering, Tianjin University of Technology and Education, Tianjin 300222, China*

ABSTRACT: This paper proposes a broadband dual-polarized (DP) magneto-electric dipole antenna (MEDA) loaded with parasitic elements. The antenna structure comprises a rectangular reflecting cavity, four corner-truncated and optimized horizontal electric dipoles, eight vertically arranged magnetic dipoles, and four triangular parasitic elements embedded in the truncated corners of the electric dipoles. An orthogonal Γ-shaped feeding network is employed to excite dual-polarized modes, ensuring stable bandwidth and gain performance. Experimental measurements demonstrate an overlapping impedance bandwidth ($|S_{11}|$ and $|S_{22}| \leq -10$ dB) of 84.7% (1.92–4.74 GHz) for both ports, with an in-band peak gain of 11.69 dBi and port isolation exceeding 27 dB. This design provides a compact high-isolation dual-polarized antenna solution for 5G multi-band communication systems.

1. INTRODUCTION

With the continuous development of wireless communication technology, higher demands are placed on high-speed and high-capacity transmission. Dual-polarized antennas, due to their orthogonal polarization characteristics, can effectively reduce multipath interference, improve channel capacity, and support multiple-input multiple-output (MIMO) technology, leading to their widespread application in wireless communication systems in recent years.

In 2006, an MEDA based on the complementary principle was designed [1]. This antenna used vertical metal plates and horizontal radiating patches to form magnetic and electric dipoles, respectively, and employed a Γ-shaped probe for coupling feed. The radiation pattern of the electric dipole in such antennas resembles the number "8" in the E-plane and the letter "O" in the H-plane. Conversely, the magnetic dipole's pattern appears as the letter "O" in the E-plane and the number "8" in the H-plane, demonstrating significant complementarity in their radiation patterns. Additionally, these antennas exhibit characteristics such as wide bandwidth, high gain, and low cross-polarization levels. In 2008, a new variant of DP-MEDA was introduced [2], which achieved an overlapping impedance bandwidth of 65.9% across its two ports and a maximum gain of 9.5 dBi. With further research, scholars have conducted extensive studies on low-profile, high-isolation, and wideband high-gain DP-MEDAs. In [3], the impedance matching of an antenna was enhanced by shaping an electric dipole into a bowtie configuration. Ref. [4] utilized a small-gap equilateral triangular cavity as the magnetic dipole, leading to a lower antenna profile. Ref. [5] designed a broadband high-isolation MEDA using low-temperature co-fired ceramic technology, achieving over 55 dB isolation by leveraging anti-phase coupling from the grounded feed slot to another excitation port. Ref. [6] achieved a low profile of $0.1\lambda_0$ (λ_0 is the free-space wavelength at the center frequency) and 40% impedance bandwidth using multilayer dielectric integration and microstrip slot-coupled feeding technology. Ref. [7] significantly enhanced the antenna gain across the operating band by loading a director above the radiator. Refs. [8, 9] optimized the feeding structure. Refs. [10–13] introduced parasitic structures to achieve outstanding bandwidth and gain. However, these antennas exhibit complex structures, incur high manufacturing costs, and demonstrate high sensitivity to environmental interference, making them prone to interference from nearby metallic structures or other wireless devices, which adversely affects their performance.

To address the aforementioned issues, this paper proposes a wideband DP-MEDA loaded with parasitic elements. The antenna features chamfered horizontal metal plates, and the width of the vertical metal plates of the radiator is adjusted based on the chamfer length. An orthogonal Γ-shaped feeding structure is used to excite the antenna, and by incorporating triangular parasitic elements, the design achieves stable bandwidth and gain while maintaining a compact structure.

2. ANTENNA STRUCTURE AND DESCRIPTION

As shown in Figure 1, the proposed wideband DP-MEDA loaded with parasitic elements consists of four parts: a rectangular reflecting cavity, a magneto-electric dipole radiator, an orthogonal Γ-shaped probe feed, and parasitic elements. The rectangular reflecting cavity has a length of G_b and height of G_h. The orthogonal Γ-shaped probe feeding structure consists of Probe 1 and Probe 2, orthogonally positioned at the center of the rectangular reflecting cavity. The magneto-electric dipole radiator consists of four identical radiating elements, which are vertically placed around the orthogonal Γ-shaped probe feed,

* Corresponding author: Wusheng Ji (jiwusheng@tute.edu.cn).

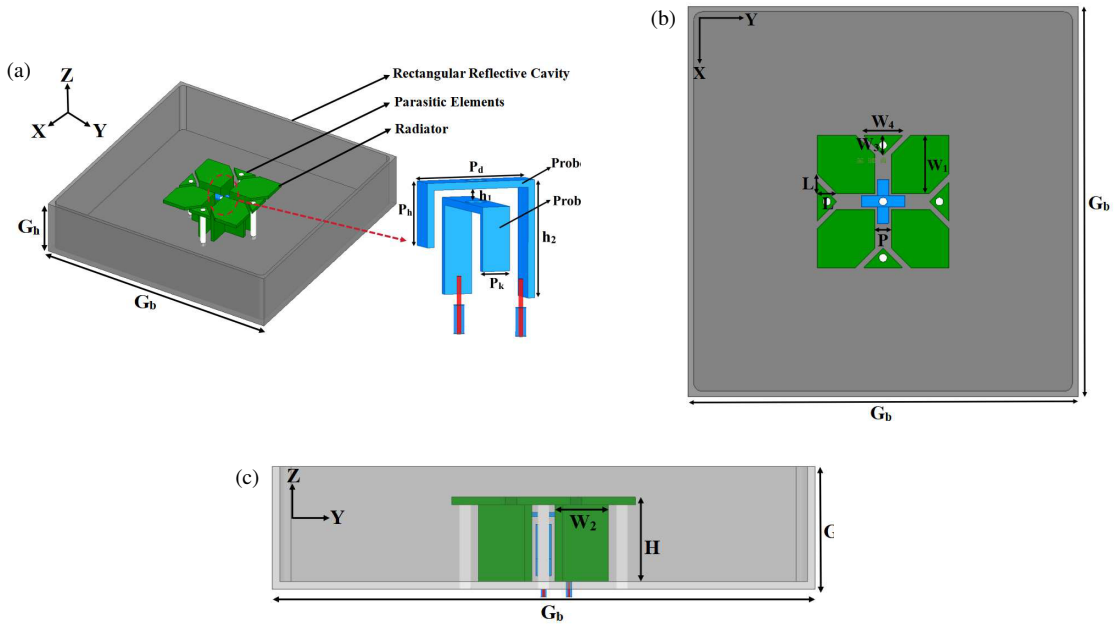

FIGURE 1. Schematic diagram of the antenna structure. (a) Three-dimensional view of the antenna; (b) Antenna top view; (c) Front view of the antenna.

forming four pairs of 360° rotationally symmetric magneto-electric dipole radiators. The distance among the four radiating elements is P. Each radiating element comprises a horizontal metal plate and two vertical rectangular metal plates. The rectangular plates are vertically aligned along the inner edges of the horizontal plate. The horizontal plate, with both length and width of W_1, is positioned at a height H above the ground plane of the rectangular reflecting cavity, with two isosceles right triangles of side length L removed. The rectangular plates have a width of W_2 and a height of H. The parasitic unit consists of four triangular metal plates with a base length of W_4 and height of W_3. These plates are centrally positioned within the chamfered gaps of the four horizontal electric dipole metal plates, secured to the rectangular reflecting cavity via nylon screws at a height H above the ground plane. Detailed antenna dimensions are provided in Table 1.

TABLE 1. Antenna dimension parameters.

Parameters	G_b	G_h	P	P_d	P_h	P_K	W_1
Value (mm)	142	30	6	16	9	4	21
Parameters	W_2	W_3	W_4	H	h_1	h_2	L
Value (mm)	14	7	14	22	3	18	7

3. ANTENNA ANALYSIS

3.1. Antenna Design Process

As shown in Figure 2, the design evolution process of the antenna proposed in this paper is illustrated. The reflection coefficient and gain curves of the three antennas are shown in Figure 3, where the left vertical axis represents the reflection coefficient, and the right vertical axis represents the antenna gain. Antenna 1 is a traditional DP-MEDA structure with an impedance bandwidth ($|S_{11}| \leq -10$ dB) of 68.4% (2.26–4.61 GHz) and a maximum in-band gain of 10.74 dBi. By chamfering the horizontal metal plate of the Antenna 1 radiator and optimizing the width of the vertical metal plates accordingly, Antenna 2 was obtained. As shown in the reflection coefficient curve of Figure 3, Antenna 2 exhibits a reflection coefficient exceeding -10 dB in the mid-frequency band, indicating impedance mismatch. Building upon Antenna 2's radiator configuration, Antenna 3 was developed by integrating triangular parasitic elements into the chamfered gaps of the horizontal metal plates across four radiators. This antenna achieves an impedance bandwidth ($S_{11} \leq -10$ dB) of 85% (1.95–4.83 GHz) with a maximum in-band gain of 12.28 dBi. The reflection coefficient and gain curves in Figure 3 demonstrate that the introduction of the parasitic elements optimizes the antenna's impedance matching, achieving stable bandwidth

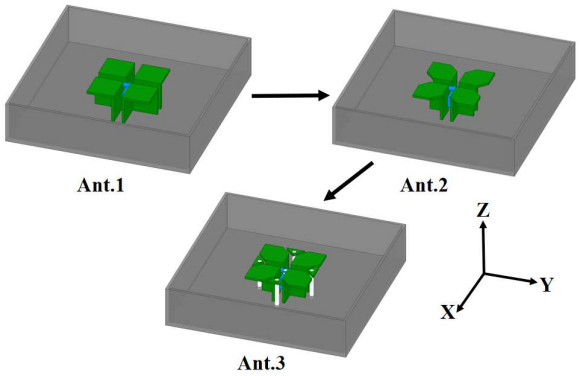

FIGURE 2. Evolution of antenna design plot.

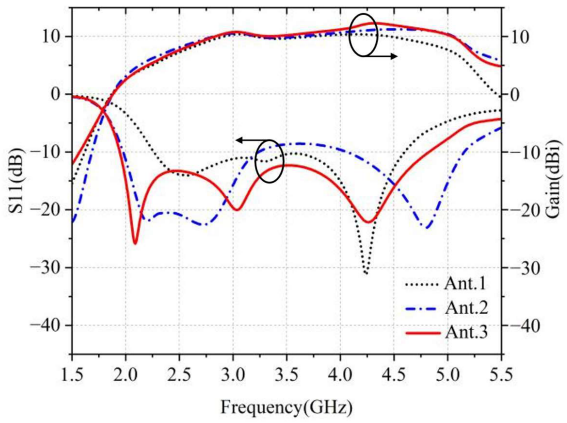

FIGURE 3. Comparison of reflection coefficients and gains of three antennas.

and gain within the operating frequency band, thereby endowing the proposed antenna with excellent performance.

3.2. Working Principle of the Proposed Antenna

Figure 4 illustrates the equivalent circuit models of the magnetic dipole and electric dipole [14]. Herein, the parallel LC circuit represents the magnetic dipole, while the series LC circuit corresponds to the electric dipole. When these two resonant circuits are connected in parallel, the input admittance of the equivalent circuit is given by Equation (1).

$$Y_{in} = \left[\frac{1}{R_e} + \frac{1}{R_m}\right] + j\left[\left(\omega L_e - \frac{1}{\omega C_e}\right)\frac{1}{R_e^2} - \left(\omega C_m - \frac{1}{\omega L_m}\right)\right] \quad (1)$$

where ω denotes the antenna's operating frequency, when both magnetic and electric dipoles achieve resonance at the same frequency point, the resonant frequencies of the magnetic dipole's parallel oscillating circuit and electric dipole's series oscillating circuit become identical. This leads to the imaginary part of the above equation being zero, yielding:

$$C_e L_e = C_m L_m \quad (2)$$

$$R_e^2 = \frac{L_e}{C_m} \quad (3)$$

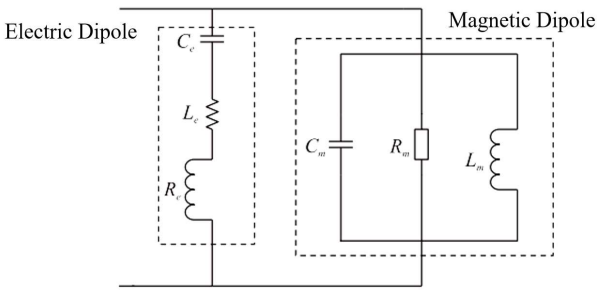

FIGURE 4. Equivalent circuit of magnetoelectric dipole.

From the perspective of the entire circuit, the synergistic interaction between magnetic and electric dipoles enables the antenna to exhibit stable equivalent impedance characteristics over a broad frequency range, which contributes to achieving exceptional bandwidth and gain performance. Under ideal resonance conditions, the imaginary component of the antenna's input admittance can be reduced to zero, indicating that the circuit has attained an optimal resonant state.

DP-MEDA is based on the orthogonal structure and electromagnetic complementary characteristics of electric dipole and magnetic dipole. The electric dipole usually adopts a pair of metal patches, forming dipole current distribution under excitation, mainly producing directional electric field radiation, while the magnetic dipole uses shorted metal walls or loop structures to form magnetic current loops, producing magnetic field radiation, whose electromagnetic complementary characteristics make the E-plane and H-plane radiation patterns show good symmetry. By orthogonally arranging two pairs of electric and magnetic dipole structures and independently feeding them, two orthogonally polarized radiation modes can be formed to achieve the DP characteristics of the antenna.

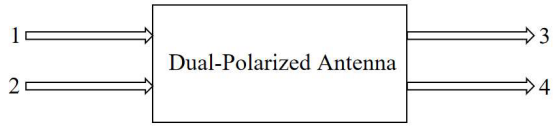

FIGURE 5. Four-port network circuit of dual-polarized antenna.

Figure 5 shows the four-port network circuit of the DP antenna. DP generally refers to two mutually orthogonal polarizations. The orthogonal radiation from the two ports of DP can form multiple independent channels in communication, reducing signal fading and increasing channel capacity. Port 1 in the figure represents radiation in one polarization direction, while Port 3 represents radiation in the orthogonal direction to this polarization. Port 2 represents radiation in another polarization direction, and Port 4 represents radiation in the direction orthogonal to this polarization. When the two feeding ports of the DP antenna operate separately, S_{11} indicates the return loss at one input port, and S_{22} indicates the return loss at the other input port. These two parameters respectively represent the return loss between different ports. The isolation between the two ports of the DP antenna is represented by S_{12} and S_{21}.

At 3.3 GHz, the simulated surface electric field distribution of the antenna radiating patch is shown in Figure 6. Figure 6(a) shows the surface electric field distribution when port 1 is excited, and Figure 6(b) shows the surface electric field distribution when port 2 is excited. From Figure 6(a), it can be observed that at $t = 0$, the current is mainly distributed along the edges of the radiating patch slots in the X-axis direction, and at this time the radiator operates in magnetic dipole mode; at $t = T/4$, the electric field distribution is stronger across the entire radiator surface, and at this time the radiator operates in electric dipole mode. From Figure 6(b), it can be observed that under port 2 excitation at $t = 0$, the electric field around the Y-axis directional slots on the radiator surface is very strong, indicating magnetic dipole mode; at $t = T/4$, the electric field distribu-

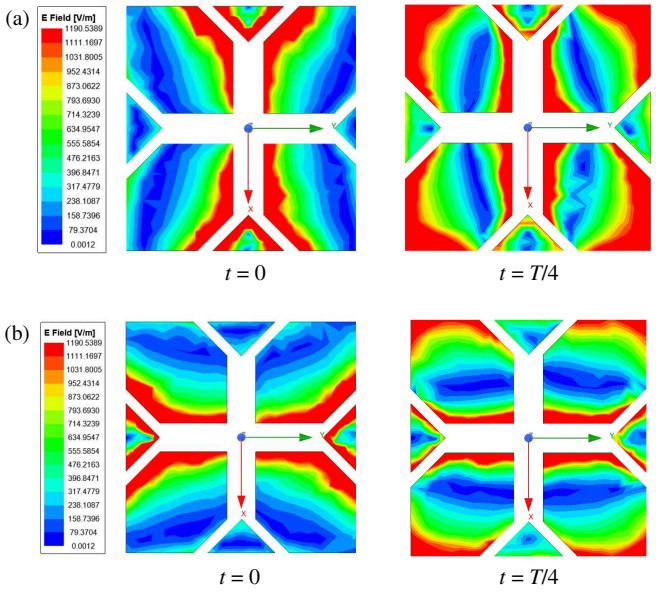

FIGURE 6. Surface electric field distribution simulated by antenna radiation patch at 3.3 GHz, (a) port 1; (b) port 2.

tion across the entire radiator surface becomes stronger, demonstrating electric dipole mode. Therefore, this antenna can be observed at both ports to alternately operate in two dipole modes within each cycle, while maintaining a 90° phase difference excitation, consistent with the complementary characteristics of MEDA. Meanwhile, by loading triangular parasitic elements at the gaps of the horizontal electric dipole metal plates, the surface electric field distribution is optimized, reducing edge current scattering loss and thereby improving antenna radiation efficiency.

3.3. Key Parameter Study of the Antenna

To thoroughly analyze the impact of key antenna parameters on its performance, this paper conducts detailed parameter scanning using the electromagnetic simulation software HFSS. The antenna employs an orthogonally placed Γ-shaped probe feeding structure, with Port 1 and Port 2 exhibiting similar parameter characteristics. Therefore, this paper only presents the parameter scanning results for Port 1 operation, while the corresponding results for Port 2 operation are not shown.

L represents the side length of the chamfered corner of the horizontal metal plate in the proposed antenna radiator. The impact of varying L on antenna performance is shown in Figure 7. From the reflection coefficient curves in the figure, it can be observed that as L increases, the curves gradually shift toward higher frequencies. When $L = 8$ mm, the antenna exhibits impedance mismatch around 3.5 GHz. Therefore, considering the overall impedance matching of the antenna, the best matching effect is achieved at $L = 7$ mm, with an impedance bandwidth of up to 85%.

W_3 represents the height of the triangular parasitic element in the proposed antenna. Since the triangle is isosceles, both its height and base length affect the reflection coefficient. However, since the base length W_4 changes together with the height W_3, only the influence of W_3 on the reflection coefficient is

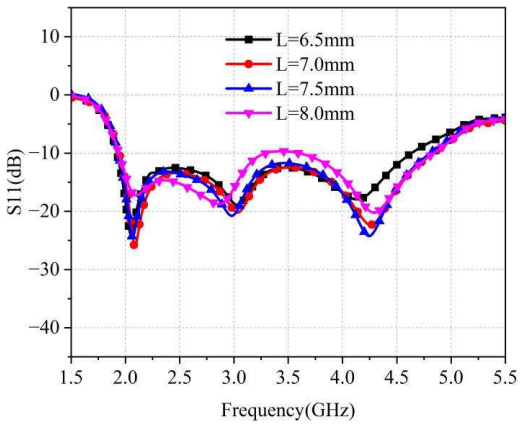

FIGURE 7. The influence of parameter L on reflection coefficient.

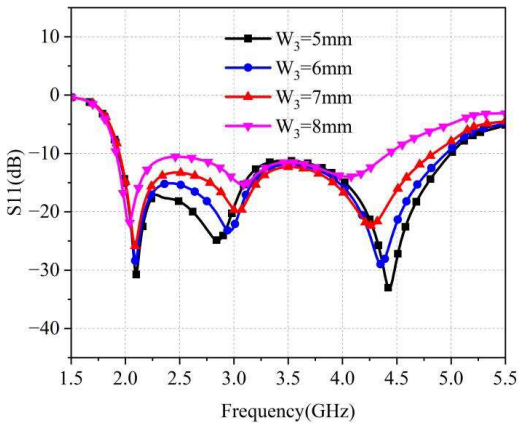

FIGURE 8. The influence of parameter W_3 on reflection coefficient.

shown here, as illustrated in Figure 8. From the reflection coefficient curves in the figure, it can be observed that as W_3 increases, the impedance bandwidth gradually decreases. It can also be observed that the antenna exhibits a wider impedance bandwidth when $W_3 = 6$ mm. However, around the center frequency of 3.3 GHz, the antenna with $W_3 = 7$ mm demonstrates better impedance matching across the entire operating band. Therefore, considering both the impedance matching performance and the practical fabrication of the antenna, $W_3 = 7$ mm is selected.

4. ANTENNA FABRICATION AND MEASUREMENT RESULTS

4.1. Antenna Fabrication

The proposed antenna model was fabricated using precision machining, and its performance parameters were measured in a microwave anechoic chamber. As shown in Figure 9, the antenna prototype consists of a rectangular reflecting cavity, a magneto-electric dipole radiator, and triangular parasitic elements, all made of 2 mm thick aluminum plates, while the Γ-shaped probe is fabricated from 1 mm thick copper sheets. The triangular parasitic elements are secured to the rectangular reflecting cavity with 1.5 mm radius nylon studs, and the probe base is linked via an SMA connector, ensuring conve-

FIGURE 9. Photograph of the antenna prototype.

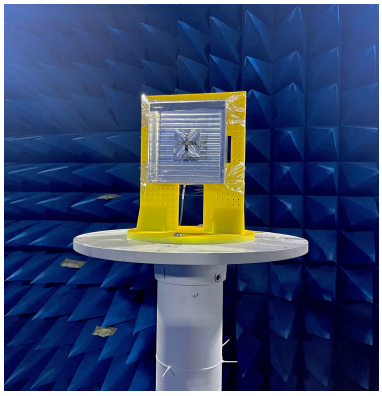

FIGURE 10. Photograph of microwave anechoic chamber measurement.

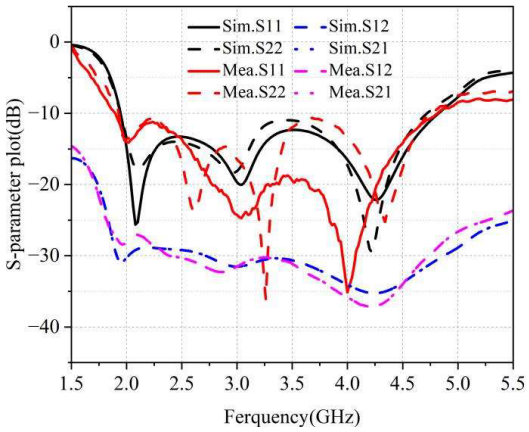

FIGURE 11. Simulated and measured S-parameter plots.

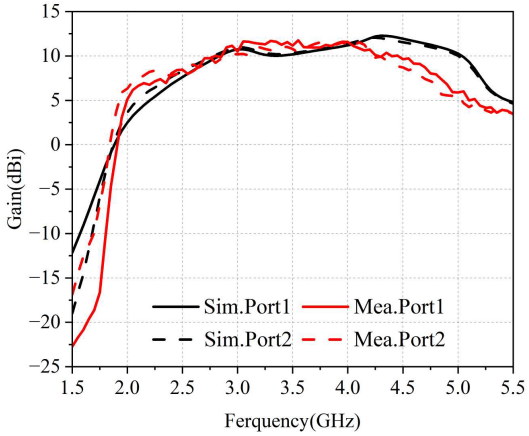

FIGURE 12. Simulated and measured gain plots.

nient assembly and disassembly of the antenna components. Figure 10 shows the antenna measurement in a microwave anechoic chamber.

4.2. Antenna Measurement Results

The measured and simulated results of the proposed antenna are shown in Figure 11. The simulated impedance bandwidths ($|S_{11}|$ and $|S_{22}| \leq -10$ dB) for the two ports are 85% (1.95–4.83 GHz) and 83.1% (1.95–4.72 GHz), respectively. The measured impedance bandwidths ($|S_{11}|$ and $|S_{22}| \leq -10$ dB) are 86.9% (1.9–4.82 GHz) and 84.7% (1.92–4.74 GHz), respectively. The overlapping bandwidths between measurement and simulation are 84.7% (1.92–4.74 GHz) and 83.1% (1.95–4.72 GHz), respectively. Across the operating frequency range, the port isolation exceeds 27 dB. The measured and simulated gains are shown in Figure 12. The measured peak gains for the two ports are 11.69 dBi and 11.51 dBi, respectively. Despite limitations in machining precision, the measurement results demonstrate good agreement with simulations, indicating practical applicability.

The measured and simulated radiation patterns at 2.6 GHz, 3.3 GHz, and 4.0 GHz are shown in Figure 13. The measured and simulated radiation patterns demonstrate good agreement, with both E-plane and H-plane patterns exhibiting excellent symmetry, aligning with the radiation characteristics of MEDA. Within the operating frequency range, the measured and simulated front-to-back ratios of the proposed antenna both exceed 20 dB. The cross-polarization levels in the E-plane and H-plane are below -20 dB. Therefore, the proposed dual-polarized antenna exhibits excellent radiation characteristics.

A performance comparison between the proposed antenna and previously published DP-MEDAs is presented in Table 2. Ref. [15] achieved a low-profile design using composite dielectric and metal patches, but the realized impedance bandwidth is narrow. Moreover, the precise stacking structure of composite dielectric and metal patches increases fabrication complexity and production costs. Ref. [16] reduced electromagnetic wave scattering and enhanced far-field radiation by optimizing the magneto-electric dipole radiator structure and integrating a rectangular reflecting cavity, achieving stable bandwidth and gain. However, the dual-polarized antenna proposed in this work demonstrates more competitive bandwidth and gain performance. Ref. [17] introduced annular slots on the ground plane to implement filtering functionality, reducing insertion loss and overall size. However, its peak gain of merely 7 dBi fails to meet the high-gain requirements of modern communication systems. Ref. [18] introduced four symmetrical rectangular slots to the traditional dual-polarized magneto-

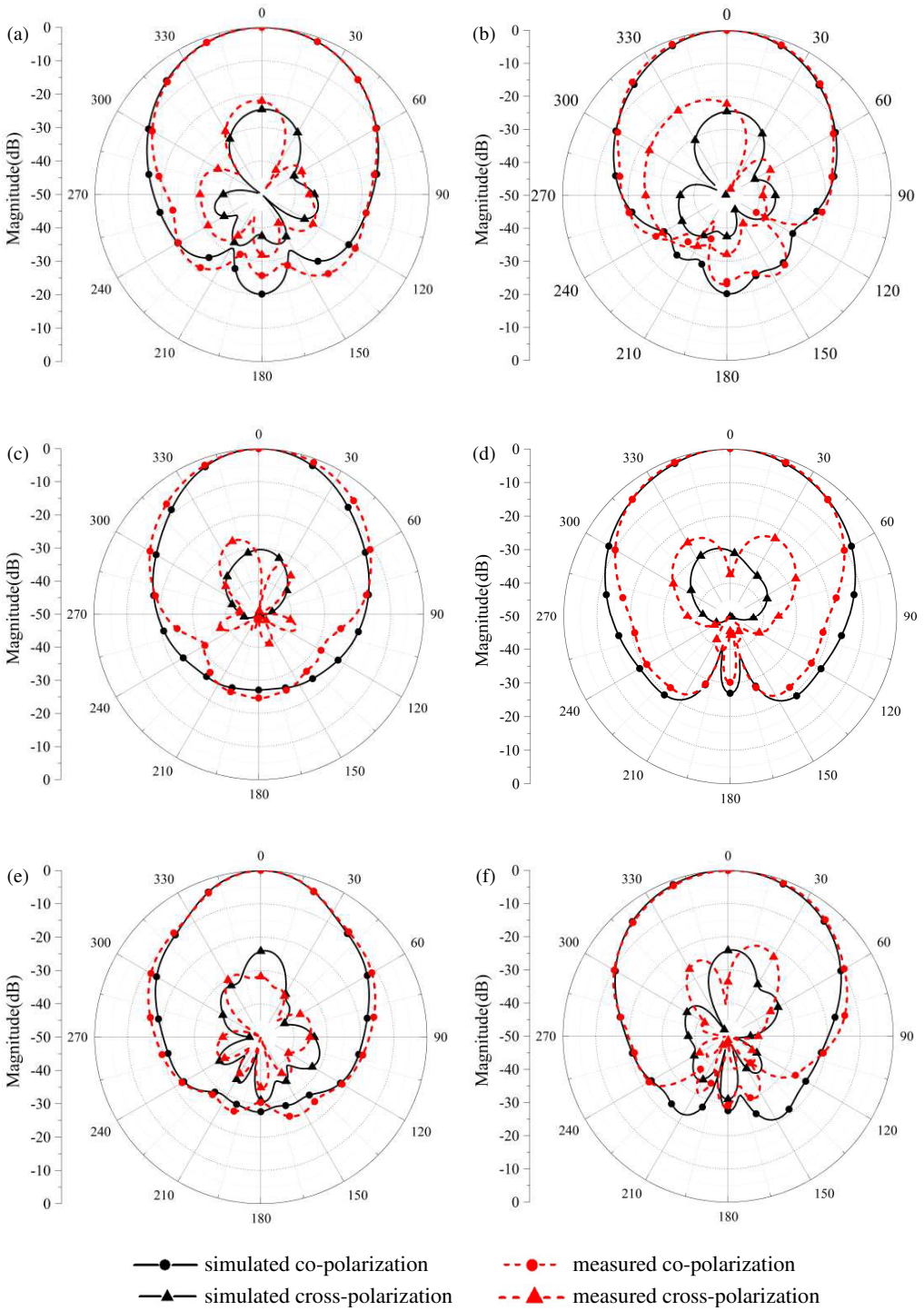

FIGURE 13. Simulated and measured radiation patterns of the antenna. (a) E-plane at 2.6 GHz; (b) H-plane at 2.6 GHz; (c) E-plane at 3.3 GHz; (d) H-plane at 3.3 GHz; (e) E-plane at 4.0 GHz; (f) H-plane at 4.0 GHz.

electric dipole and improved the Γ-shaped probe structure to make the antenna more compact. However, the complex radiator and probe design increased the difficulty of mechanical fabrication. Ref. [19] optimized the traditional magneto-electric dipole structure and incorporated parasitic elements, achieving an impedance bandwidth of 101.7% and a high gain of 11.5 dBi. However, the proposed antenna in this work demonstrates superior frequency coverage and port isolation.

In summary, the proposed wideband DP-MEDA with parasitic elements demonstrates excellent performance, achieving extended operating bandwidth while maintaining gain stability. However, due to the small size of the parasitic elements, the required mechanical fabrication precision is increased. Further research is needed to optimize the parasitic element structure and reduce the antenna's manufacturing complexity.

TABLE 2. The antenna proposed is compared to other antennas.

Ref.	Size (λ_0^3)	Frequency Band (GHz)	Overlapped BW (%)	Peak Gain (dBi)	Isolation (dB)
[15]	$0.61 \times 0.61 \times 0.09$	3.3–4.0	19.2	7.5	-20
[16]	$0.82 \times 0.82 \times 0.16$	3.2–6.6	69	10.3	-25
[17]	$1.02 \times 1.02 \times 0.27$	1.55–3.54	78.03	7	-17
[18]	$0.57 \times 0.57 \times 0.16$	3.06–5.28	53.2	9.6	-22
[19]	\	1.18–3.62	101.7	12.5	-20
This work	$1.56 \times 1.56 \times 0.33$	1.92–4.74	84.7	11.69	-27

5. CONCLUSION

This paper proposes a wideband DP-MEDA with loaded parasitic elements. The DP antenna employs orthogonally arranged Γ-shaped feeding structures to drive improved magneto-electric dipole radiators integrated with parasitic elements, thereby attaining stable operational bandwidth and high port isolation. Measurement results show that the overlapping impedance bandwidth ($|S_{11}|$ and $|S_{22}| \leq -10$ dB) for both ports is 84.7% (1.92–4.74 GHz), with an in-band peak gain of 11.69 dBi and port isolation greater than 27 dB. Therefore, this DP antenna demonstrates promising application prospects in wireless communications, radar systems, and satellite communications.

ACKNOWLEDGEMENT

This work is supported by Tianjin Key Projects of Research and Development and Science and Technology Support in 2020 (20YFZCGX00700), and Tianjin Enterprise Science and Technology Commissioner Project in 2022 (22YDTPJC00330).

REFERENCES

[1] Luk, K.-M. and H. Wong, "A new wideband unidirectional antenna element," *International Journal of Microwave and Optical Technology*, Vol. 1, No. 1, 35–44, 2006.

[2] Wu, B. Q. and K.-M. Luk, "A broadband dual-polarized magneto-electric dipole antenna with simple feeds," *IEEE Antennas and Wireless Propagation Letters*, Vol. 8, 60–63, 2008.

[3] Wong, H., K.-M. Mak, and K.-M. Luk, "Wideband shorted bowtie patch antenna with electric dipole," *IEEE Transactions on Antennas and Propagation*, Vol. 56, No. 7, 2098–2101, Jul. 2008.

[4] Ding, C. and K.-M. Luk, "A low-profile dual-polarized magneto-electric dipole antenna," *IEEE Access*, Vol. 7, 181 924–181 932, 2019.

[5] Yang, K. Y., W. J. Zhu, L. H. Ye, J.-F. Li, and D.-L. Wu, "LTCC-based wideband dual-polarized magneto-electric dipole antenna array with high isolation," in *2022 IEEE MTT-S International Microwave Workshop Series on Advanced Materials and Processes for RF and THz Applications (IMWS-AMP)*, 1–3, Guangzhou, China, 2022.

[6] Liang, M.-S., Y. Zhou, X.-S. Yang, and P.-F. Wu, "A low-profile dual-polarized substrate integrated magneto-electric dipole MIMO antenna," *IEEE Antennas and Wireless Propagation Letters*, Vol. 22, No. 6, 1431–1435, Jun. 2023.

[7] Feng, L. Y. and C. Q. Zhang, "Compact magneto-electric dipole director loaded high-gain dual-polarized magneto-electric dipole antenna," *IEEE Antennas and Wireless Propagation Letters*, Vol. 23, No. 7, 2130–2134, Jul. 2024.

[8] Chu, Z., Y. Yu, Q. Chen, Z. Qian, and W. Wu, "A wideband millimeter-wave dual-polarized magneto-electric dipole antenna with a high isolation level," in *2023 16th UK-Europe-China Workshop on Millimetre Waves and Terahertz Technologies (UCMMT)*, 1–3, Guangzhou, China, 2023.

[9] Xi, Y., Y. Wang, H. Zhai, and C. Liu, "A broadband dual-polarized filtering base-station antenna for 5G communication applications," *Microwave and Optical Technology Letters*, Vol. 64, No. 5, 911–917, May 2022.

[10] Behboudi, M., J. Nourinia, and C. Ghobadi, "Miniaturized printed X-band magneto-electric dipole antenna by loading parasitic elements," in *2024 11th International Symposium on Telecommunications (IST)*, 561–566, Tehran, Iran, 2024.

[11] Zhou, B., T. Wu, Z.-Y. Zhang, C. Zhou, and A. Chen, "A wideband dual-polarization magneto-electric dipole antenna with low-profile and high-gain," in *2023 IEEE 11th Asia-Pacific Conference on Antennas and Propagation (APCAP)*, 1–2, Guangzhou, China, 2023.

[12] Sun, G.-H., K. Wang, and L. W. Qin, "Design of a dual-polarized magnetoelectric dipole with gain enhancement based on patch loading," *IEEE Transactions on Antennas and Propagation*, Vol. 73, No. 1, 606–610, Jan. 2025.

[13] Huang, K. and Y. Zhang, "Analysis and design of dual-polarized millimeter-wave filtering magneto-electric dipole antenna," *IEEE Transactions on Antennas and Propagation*, Vol. 71, No. 8, 6947–6952, Aug. 2023.

[14] Luk, K.-M. and B. Wu, "The magnetoelectric dipole — A wideband antenna for base stations in mobile communications," *Proceedings of the IEEE*, Vol. 100, No. 7, 2297–2307, Jul. 2012.

[15] Chen, J.-X., T.-Y. Yan, J.-Y. Yang, and L.-L. Yang, "Dual-polarized dual magnetoelectric dipole antenna based on composite dielectric and metallic patches," *IEEE Antennas and Wireless Propagation Letters*, Vol. 23, No. 12, 4827–4831, Dec. 2024.

[16] Yang, L., K. Zhang, and Y. Luo, "Broadband dual-polarized magnetoelectric dipole antenna for 5G microcell base station," in *2024 IEEE International Students' Conference on Electrical, Electronics and Computer Science (SCEECS)*, 1–3, Bhopal, India, 2024.

[17] Liu, T., K. Y. Yang, L. H. Ye, and D.-L. Wu, "Wideband dual-polarized filtering magneto-electric dipole antenna," in *2022 IEEE MTT-S International Microwave Workshop Series on Advanced Materials and Processes for RF and THz Applications (IMWS-AMP)*, 1–3, Guangzhou, China, 2022.

[18] Wu, S. and F. Shang, "Broadband dual-polarized magnetoelectric dipole antenna with compact structure for 5G base station," *IEEE Access*, Vol. 11, 20 806–20 813, 2023.

[19] Yan, Y., Y. Xu, and A. Wang, "Design of a broadband dual-polarized magnetoelectric dipole antenna for 3G/4G/5G communication," in *2023 IEEE International Workshop on Electromagnetics: Applications and Student Innovation Competition (iWEM)*, 4–6, Harbin, China, 2023.